DG-Mapping: A novel software package for the analysis of any type of reentry and focal activation of simulated, experimental or clinical data of cardiac arrhythmia.

Enid Van Nieuwenhuyse^a, Sander Hendrickx^a, Robin Van den Abeele^a, Lars Lowie^a, Sebastien Knecht^b, Mattias Duytschaever^b, Nele Vandersickel^a

^{a}Department of Physics and Astronomy, Ghent University, Ghent, Belgium
^{b}AZ Sint-Jan, Cardiology Department, Bruges, Belgium

Abstract

In this work we present the release of a novel easy-to-use software package called DGM or Directed-Graph-Mapping. DGM can automatically analyze any type of arrhythmia to find reentry or focal sources, if the measurements are synchronized in time. Currently, DGM requires the local activation times (LAT) and the spatial coordinates of the measured electrodes. However, there is no requirement for any spatial organization of the electrodes, allowing to analyze clinical, experimental or computational data. DGM creates directed networks of the activation, which are analyzed with fast algorithms to search for reentry (cycles in the network) and focal sources (nodes with outgoing arrows). DGM has been mainly optimized to analyze atrial tachycardia, but we also discuss other applications of DGM demonstrating its wide applicability. The goal is to create a community used software package which can allow researchers to save time in the analysis of cardiac data. An academic license it attached to the software, allowing only non-commercial use of the software. All updates of the software, user and installation guide will be published on a dedicated website `wwww.dgmapping.com`.

1 Introduction

1.1 Different types of arrhythmias and sources

One possible treatment for curing an arrhythmia is via catheter ablation, which aims to restore the normal rhythm by destroying a part of the tissue. For this, it is important to determine the source and the location of the arrhythmia. It is important to destroy as little tissue as possible, since the larger the ablated area, the higher the risk of severe complications and reconnected tissue [1].

In general, there are two possible sources for an arrhythmia: reentry and triggered activity. The first driving source reentry is usually subdivided in two categories: anatomical reentry and functional reentry. Anatomical reentry occurs when the electrical wave starts to rotate around an obstacle, e.g. around a valve, a vein or scar tissue. Depending on the size of the smallest rotation, one can make a distinction between macro reentry (large obstacle, like a valve or a vein) or localized reentry (small obstacle, usually scar tissue, also called micro reentry). However, reentry is also possible without an obstacle, whereby the wave rotates around an excitable core, namely functional reentry. Functional reentry is also often called a spiral wave or a rotor. The second driving source is triggered activity or automaticity. The latter mechanism gives rise to focal activation, most likely accompanied by a concentric activation pattern.

We can divide most arrhythmia in two different types: the regular arrhythmia, called tachycardia, and the irregular arrhythmia, called fibrillation (except for Torsade de Pointes) as they make the atrial of ventricular walls fibrillate and therefore not contract regularly. When including the location of the arrhythmia, we distinguish 4 main types of arrhythmia: atrial tachycardia (AT) (e.g. atrial flutter), atrial fibrillation (AF), ventricular tachycardia (VT) and ventricular fibrillation (VF). A tachycardia can have two mechanisms, a regular reentry or a regular single focal source [2, 3]. For AT and VT, the reentry is usually reported to be anatomical, although it might be difficult to differentiate a small localized reentry from a functional reentry [4]. This is in contrast with fibrillation, which can be any combination of multiple irregular sources: reentries and focal sources which appear irregularly in the heart. For paroxysmal AF, Haissaguerre et al. [5] suggested it is triggered by irregular ectopic activity originating in the pulmonary veins region and demonstrated that pulmonary vein isolation is an effective way to manage paroxysmal AF. For persistent AF, the mechanism is still unclear, leading to a success

rate in the range of only ~50% [6, 7, 8]. Many different mechanisms have been proposed, which were recently summarized by Roney et al. [9]. All of these theories have been reported in experimental/clinical work, but were also reproduced in computer simulations. Among them are the multiple wavelet theory [10, 11, 12, 13], the motor rotor fibrillation [14, 15], the multiple rotor theory where the rotors are stable [16, 17, 18, 19] or meandering [20, 21, 19, 22], the double layer hypothesis [23, 24, 25, 26] and micro-anatomic intramural reentry [27, 28]. In addition for VF, the mechanism remains unclear, even though in the US alone VF (and VT) is responsible for about 700.000 death each year. Similarly as in AF, there exist multiple hypothesis. According to Krummen et al, VF can be divided in the following four stages: initiation, transition, maintenance and evolution [29]. VF is usually initiated by premature ventricular complexes [30] or nonsustained VT [29]. In the next three stages VF can be maintained by wandering wavelets of disorganized activity [31, 32], by mother rotor fibrillation [14], by rotors [31, 32], focal activity [31, 32]. Notice many similarities with AF, although the ventricles have the additional complexity of extra wall thickness.

1.2   Measuring an arrhythmia

In order to better understand the mechanism of an arrhythmia or to perform more precise ablation procedures, it is necessary to analyze the electrical activity in detail. In the clinic, this is done by inserting a catheter in the heart. If the arrhythmia is regular and tolerable by the patient, this can be done consecutively and many data points can be gathered. This is in contrast with an irregular arrhythmia, where it is necessary to simultaneously record the electrical activity, as the arrhythmia is continuously changing. As a consequence, irregular arrhythmia are often measured only partly via contact mapping, with a grid mapping catheter, or a circular catheter (like a lasso catheter). A way to have a more complete picture is via inserting a non-contact basket catheter inside the atrium or the ventricle. The downside is that usually not many electrodes are inserted providing a sparse view. In experimental studies in animals, much more is possible like inserting needle electrodes or performing optical measurements during Langendorf perfusion. Finally, computer simulations allow full control over the data, including millions of datapoints. After obtaining a dataset, the following methods exist to automatically detect functional, anatomical and focal activity.

1.3   Methods to analyze the data

First, in order to detect functional reentry or rotors, multiple methods were developed. The most popular method is phase mapping (PM), see Umapathy et al. for a review [33]. A first restriction is that PM requires a regular set of electrodes (like a 64-basket catheter, or a regular grid). PM assigns a phase to any signal per time frame, and looks for phase singularities, which is usually a set of 4 electrodes for which the phase differences add up to about 2π. Many different implementations were developed to assign the correct phase to the signal, using phase space [34], the Hilbert transform [35, 36], a sinusodal recomposition [37], or the filter method of Roney et al. [38]. Although PM is currently being used for clinical ablations of AF, AT and VT (FIRM procedure of Topera inc. [17]), many concerns have risen about the application of PM to guide ablations, mainly during AF. In Kuklik et al. [39], it was shown that at least eight electrodes are required to avoid frequent false positive PS detection due to chance. Also, it was showed that the number of detected rotors critically depends on the inter-electrode distance and parameters of the detection algorithm [39, 40, 41, 42]. In addition, noise has a big effect on the detection op phase singularities [43, 44], and far field and interpolation effects can induce permanent false rotors [45]. Many other methods have been developed to find rotors. We mention the following: the CARTOFINDER (Biosense Webster) [46], a method using electrocardiographic imaging (ECGI) [12], a method based on displaying electrogram dispersion [47, 48], a method based on the optical flow of the wavefront dynamics [49], sequential ultra high density contact activation mapping [50], a machine learning method based on the 12 lead ECGs [51], the ASAP method for a multipole diagnostic catheter [52], the ICAN method for the circular lasso catheter [53], machine learning methods for mapping electrodes [54, 55], single-signal algorithms based on instantaneous amplitude modulation (iAM) and instantaneous frequency modulation (iFM) [56], method to identify repetitive-regular activities (RRas) [57], the RADAR (Real-Time Electrogram Analysis for Drivers of Atrial Fibrillation) system [58], Noncontact Charge Density Mapping [59], novel integrated mapping technique searching for regions with repetitive–regular (RR) activations [60], Stochastic trajectory analysis of ranked signals (STAR) mapping [61], the wavefront field method [62], the electrographic flow mapping [63] . It is clear that an abundance of methods have been developed in the past years to find rotors. All of these methods have potential, but require further development or clinical testing and are often constructed for a particular type of catheter.

Second, although anatomical reentry arises often in AT and VT, there are almost no methods to analyze anatomical reentry automatically. Currently, if anatomically reentry is present during e.g. AT, the electrophysiologist (EP) has to manually analyze (often guided) color maps from CARTO (Biosense Webster), RHYTHMIA (Boston Scientific) and EnSite NavX (Abbott). Only one automatic method was previously developed by Oesterlein et al. [64], but it only identifies the critical areas and it does not show the reentry path.

Thirdly, focal activity can be easily detected as the region of earliest activation in between two consecutive beats. However, for more complex cases where reentry and focal, this method becomes more difficult. Again, FIRM can also detect focal sources [17], the method of Salmin et al. [65], the Focal Source and Trigger (FaST) computational algorithm [66] and the method of Oesterlein et al.[64].

1.4   DGM - A novel software package

Following the previous section, there is a clear need for new methods which can analyze any type of reentry mechanisms (functional and anatomical) in cardiac arrhythmia independent of type of measuring system. This is necessary for a better understanding of the mechanism of the arrhythmia as well as to guide the electrophysiologist (EP) during an ablation procedure. Also, it is important to make these methods public, allowing for a greater use and limiting the time researchers need to spend to each time re-implement existing methods [67]. Therefore, in this paper, we present an easy to use software package called Directed-Graph mapping or DGM, which can automatically analyze any type of arrhythmia to find reentry or focal sources. It is based on converting the excitation pattern of the electrical activity in a directed network and analyzing this directed network [44]. A platform independent (Windows, Mac, Linux) executable can be obtained after registration on `www.dgmapping.com`. DGM is available for investigators affiliated with a research institution or a hospital. It is important to note that the use of DGM is restricted under an academic license. DGM can be used for the analysis of clinical data, experimental data and in-silico data. In time, we will also allow researcher to obtain the source code for restricted non-commercial use only. In the next sections we will discuss the different parts of the software.

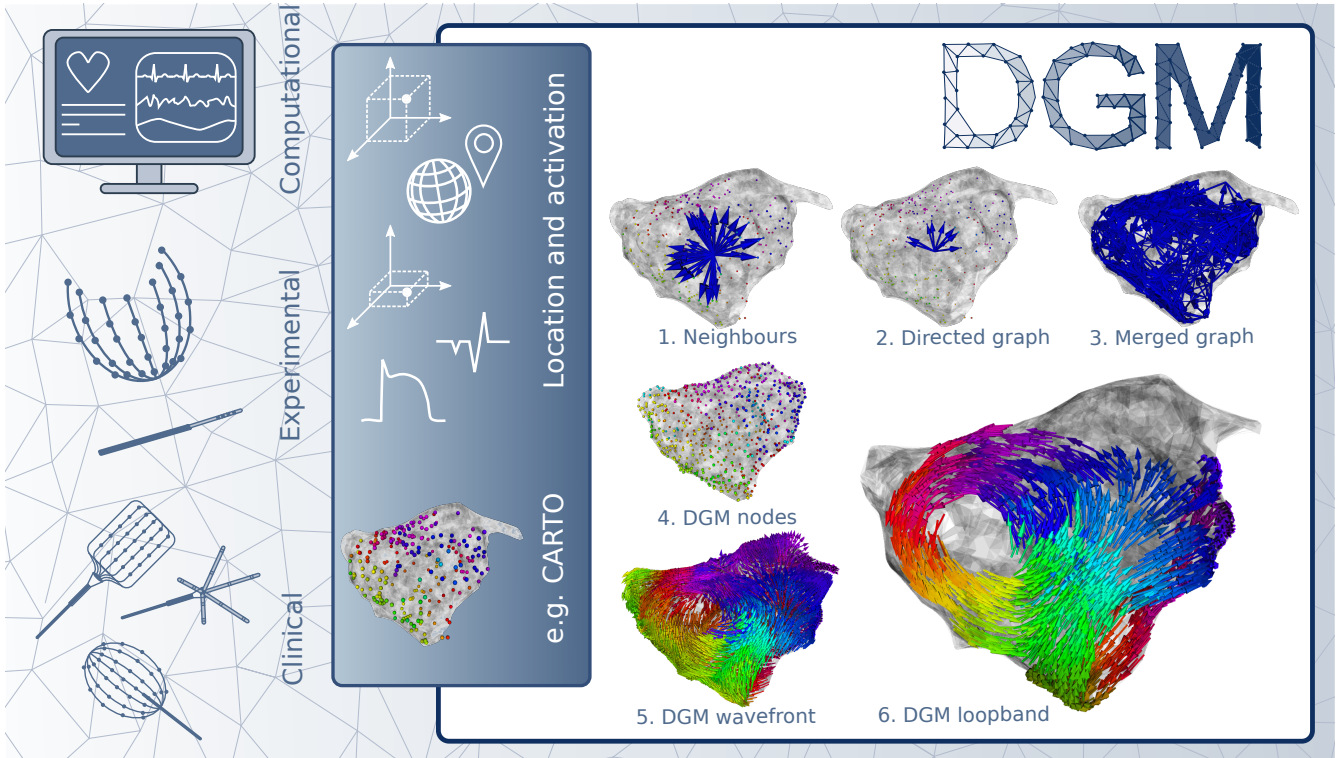# 2   General concept of DGM

Figure 1: **The concept of DGM explained.** We refer to the text for more information about the different steps.

In this section, we will provide more details on the basic concept of DGM. As explained in the previous section, DGM is based on transforming a given dataset of an arrhythmia into a directed network. It only requires a file including the spatial coordinates and the LATs of the electrodes. The LATs can be extracted from the measured signals. There is no need for any regularity of the spatial locations of the dataset, making it independent of the measuring system. Therefore, it can take as input any extracted data from a computational dataset, experimental dataset like needle data, socket data, ..., or from a clinical dataset, grid electrode data, basket catheter data, etc.

The spatial locations of the electrodes will be the nodes of the network. In the next paragraph we will explain how we will create the directed edges of the network.

2.1 Creation of the network

In Figure 1, the different steps DGM are shown [44]. First, for each electrode, the neighbours are determined using the spatial coordinates of the data points (1). A node is considered a neighbor of another node, if they are within a certain spherical distance. We currently do not take into account the geometry of the atria/ventricles to specify the neighbors. However, in a future release, we will enable a mode to read your own neighbors file, which can be created with your own algorithm. Second, for a given time t, each node's first LAT value larger than t is selected. In case of a regular arrhythmia, it can be necessary to add the cycle length to the given LAT, as only one LAT is given per node. Therefore, one should provide the correct cycle length in the GUI. Then, for each node only a directed arrow is allowed to a neighbour if the spatial distance divided by the time difference in LATs is in between a certain allowed minimal and maximal conduction velocity, see Figure 1(2). For standard parameter settings, the minimal conduction velocity is set to 0.2 mm/ms and the maximal conduction velocity is set to 2.0 mm/ms. Repeating this process for all the nodes, this creates a single directed network at a certain time t. In addition, a second network is created at a time $t + \delta t$, whereby δt is a parameter of the program, also referred to as the jump. This jump is set to 40 ms in standard settings. This second network is merged with the first network as follows. If an additional arrow is created which has the same originating LAT, it is added to the first network. This results the full directed network of excitation (3). Notice that this step is mandatory to create closed cycles in the network. As an intermediate step, the properties of this directed network are used to create more uniformly distributed nodes in case of regular datasets (4). Due to time constraints this step is currently not implemented for irregular datasets. If step 4 takes place, step (1)-(3) is repeated. Once the final network is created, DGM searches for directed cycles. In the default visualization mode, a band of loops is created for clear visualization of the reentrant pattern responsible for maintaining the arrhythmia (6). DGM also computes a wavefront representing the excitation pattern (5). In case of focal activity, the location of the focal source can be visualized by clicking on the corresponding button "focal".

2.2 Detection of re-entrant activity

To uncover the reentry loops in the arrhythmia, we search for closed cycles in the directed graph with a Breath First Search algorithm [44]. We only show the loops which have the best *variance*. This term was previously introduced in Van Nieuwenhuyse et al. [68] as phase variance. However, we choose to rename the feature as it has nothing to do with a phase and might lead to an incorrect interpretation. To concept can be explained as follows. We order the values of the LATs for each consecutive node of the cycle on the Y-axis of a graph and draw a straight line between the first and last node. The variance is the sum of the quadratic errors between the line and the actual LATs. We visualize the loops with the lowest variance. In case multiple cycles are detected, we calculate the geometrical mean of the cycle and in case the geometrical means of 2 cycles differ more than the value of the paramter Core separator, these reentries will be visualized separately. To enhance the intuitive visualization and corresponding interpretation, we have added a loopband feature, which emphasises and colors the reentry loops (6).

2.3 Detection of focal activity or automaticity

In addition to reentry loops, DGM can also find focal sources. For this, LATs are put in different bins to receive a single LAT value. This reduces unwanted variation on the LATs. Based on these new LAT values, the directed network in (1)-(3) is reconstructed. We check if regions with only outgoing arrows are present, for which the middle of these regions corresponds to the source of the focal activity [44]. The arrows pointing outwards from these regions, correspond with the propagation of the focal sources.

2.4 Regular versus irregular arrhythmia

In case DGM analyzes a regular arrhythmia, only a single network requires analysis, which agrees with a single time frame. However, in case you analyze an irregular arrhythmia, DGM will sequentially repeat the previous described steps for the complete time interval in steps provided by the user. This will allow the user to analyze the arrhythmia sequentially. More information regarding the analysis of regular data sets can be found in Vandersickel et al. [44] and Van Nieuwenhuyse et al. [68]. An example of an analysis of an irregular dataset can be found in Vandersickel et. al [69] and Van Nieuwenhuyse et al. [70].
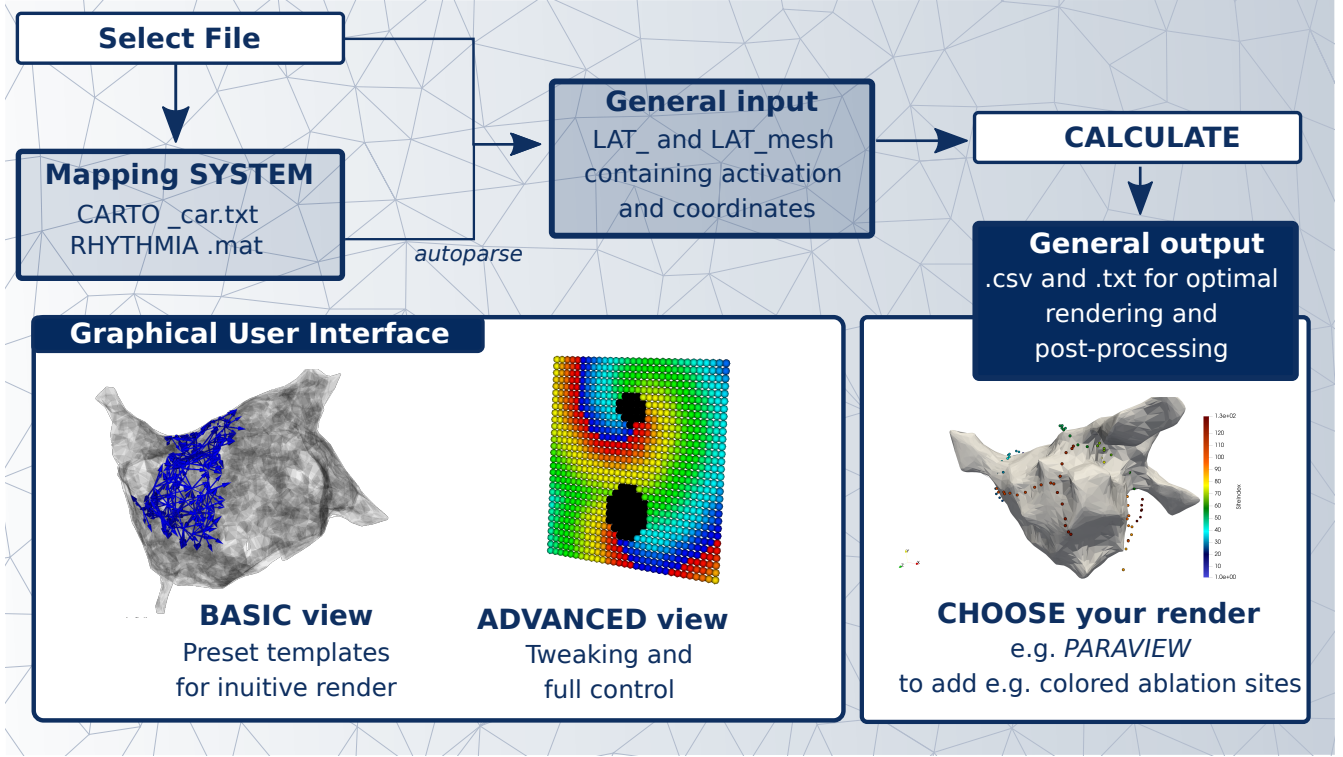
4

3 DGM software

Figure 2: **General flow of the software:** Once a file is selected, DGM checks if you wish to render a company file such as CARTO or RHTYHMIA. In that case, the files are automatically pre-processed to a standard DGM format. This general input is used for the graphical user interface to visualise the electrodes and the mesh. Once you press calculate, the C back-end creates *.csv* and *.txt* files. These files are used as an input for the visualization in the GUI (basic or advanced view, depending on the user's needs). In addition, the user can choose to change the files and visualize them in a software of choice, such as Paraview etc.

3.1 Input files

In this section, we will discuss which input files DGM can handle. In addition to a general input file format, DGM can also process the industry standards of two main mapping systems: CARTO (Biosense Webster) and RHYTHMIA (Boston Scientific). DGM will automatically preprocess these formats into the general input file format. For more information regarding the industry standard, we refer to section 3.1.2. DGM can also handle files generated by openCARP [71], an open source software package for simulating a broad variety of different arrhythmia in 2D and 3D. Once the software is opened and the input file is loaded, a copy or modification of that file will be generated in the input folder. This way, the original file will solely be used for reading remains unaltered.

3.1.1 General input file

DGM works with a standard input file format which contains (1) the spatial coordinates of the electrode recordings and (2) the annotated LATs of these electrode recordings. DGM can handle both regular arrhythmia (one LAT per location with a fixed cycle length) as irregular arrhythmia (multiple LATs per spatial location). As mentioned before, as long as the input file is in the right format, DGM is independent of the type of measuring system. Optionally, the spatial coordinates of a mesh can be included in the folder. These coordinates will be used to create a triangulated mesh in the user interface.

LAT file: obligatory
The LATs for a regular and irregular arrhythmia need to be in the following file format:

index	:	x	y	z	[LATs]
0	:	x0	y0	z0	$LAT0_1$, $LAT0_2$, $LAT0_3$, ...
1	:	x1	y1	z1	$LAT1_1$, $LAT1_2$, $LAT1_3$, ...
2	:	x2	y2	z2	$LAT2_1$, $LAT2_2$, $LAT2_3$, ...
...					

Table 1: The format of the input file for the LATs. xi, yi and zi represent the coordinates of node i, and $LATi_k$ is the kth LAT of node i. The file should be named $LAT\_p\{n\}.txt$ whereby n is the number of nodes. For example, for 250 points, the file should be named $LAT\_p250.txt$. The top line should not be included, so the user can start from node 0.

In case of a regular arrhythmia, there is only one LAT per node, and the cycle length of the arrhythmia needs to be entered in the GUI. For an irregular arrhythmia, DGM will automatically detect that there are multiple LATs for a single node in the file, so it will be impossible to enter a cycle length in the GUI. In case tissue is considered as scar or with a low voltage, one can choose to assign a -1 to these coordinates in the LAT file. Nodes which represent scar tissue will be shown as black spheres in the visualization and can be important for understanding the arrhythmia. It is important to note that the scarred regions should also be counted as nodes. So in case their are 5 scar electrodes and 200 accepted electrodes, the number of nodes in the input file has to be 205.

LAT_mesh file: optional
In case the arrhythmia is recorded with additional tools often a mesh for visualization is available. Hence we made it possible to also include the spatial positions of a mesh which needs to be placed in the same folder as the LAT file. DGM will automatically check if a coordinates mesh file is present and will load this in the GUI. The nodes present in the LAT_mesh file will be used for the generation of a grey mesh in the GUI. Important to note is that when the user will provide a mesh file, the wavefront analysis will take place on the nodes of this file, not the vertices, see section 3.2 for more information on the wavefront. In case no mesh file is provided, DGM will automatically generate a mesh from the spatial distribution of the recorded electrodes. The coordinates mesh file should have the following format:

index	:	x	y	z	LAT
0	:	x0	y0	z0	0
1	:	x1	y1	z1	0
2	:	x2	y2	z2	0
...					

Table 2: The format of the input file for the coordinates of the mesh. xi, yi and zi represent the coordinates of ith point of the mesh. The file should be named $LAT\_mesh\_p\{n\}.txt$ whereby n is the number of nodes of the electrodes, not the number of points in the mesh, which are usually higher than the number of nodes. Also a padding value of 0 needs to be added to the file. Again, the first line of the table starting with index should not be included in the file.

3.1.2 Existing mapping systems

CARTO DGM can handle the output format of the CARTO system of Biosense Webster. The latest system which was tested is CARTO 3 v7. However, older formats might have another header, in which case we will have to add another module to read this format. The mapping can be performed with single electrode ablation catheters or multi-electrode catheters like PentaRay. We have tested CARTO formats solely for the analysis of regular arrhythmias such as AT and VT. However, the CARTO system can also be used to measure the heart during sinus rhythm (SR), which can be considered a regular arrhythmia as well. In that case, DGM will currently not give any useful information for SR, although we plan to further develop DGM to extract additional structural information.

A full export of the study data of a CARTO case will generate at least two important files: a _car.txt file, which contains the LATs and the coordinates of the measured points and a .mesh file which contains all the information about the mesh of the atrium or ventricle. Both files should be in a single folder. However, if the user decides not to include the mesh, DGM will generate a mesh based on some basic algorithms, but the results will be visually less appealing. In case the $VisiTagExport/Sites.txt$ file is added to the folder, DGM will also be able to show ablation points. Additionally, in a case where the correct tags are labeled, also PPI-TCL points

can be loaded. For this, the study's *.xml* file should be put in the same folder as the *_car.txt* and mesh file. In case a PPI-TCL point is recorded and saved during the procedure, one should use the tags presented in section 3.1.4.

RHYTHMIA DGM can also process files generated by RHYTHMIA, the mapping software of Boston Scientific. Mapping can be performed with single electrode ablation catheters or multi-electrode catheters like Orion. All necessary information is merged within a single *.mat* file which contains the LAT and coordinates. The RHYTHMIA system is known for gathering a large amount of electrode recordings. DGM will use this abundance of electrode recordings to generate a mesh file as well as select a set of electrodes for the analysis of the reentry sources or focal activity.

Ensite DGM is not yet adapted to automatically parse the mapping system of Abbott for which mapping can be performed with single electrode ablation catheters or multi-electrode catheters like HD grid. In case there is a need, we will implement this mapping system in the future.

3.1.3 OpenCARP

DGM can also automatically analyze a simulation generated by openCARP. Currently, DGM can interpret the *.pts* and *.vtk* (meshes) files required for the generation of a simulation, and the *.igb* file, which contains the output of the simulation. Again, these 3 files should be located in the same folder, together with a costume written *openCARP.csv* file in a comma separated format. For clearness, we present an example of this latter file which should be adapted according to the simulation:

5 The simulation time step is 5 ms.

1000 The conversion from a mesh in units of micron to millimeter is 1000. DGM works in units of ms and mm.

1000 The number of electrodes a user would like to extract from the simulation in a 3D setting. This will be a random selection of points.

29 In case of 2D simulation, DGM will select electrodes in a grid of 29X29 electrodes.

-40.0 The voltage threshold which will be used to calculate the LAT by means of the upstroke of the action potential.

block.vtk Is the name of the vtk file.

block.pts Is the name of the pts file.

In summary, the *openCARP.csv* should look as follows

<div align="center">5, 1000, 1000, 29, -40.0, block.vtk, block.pts</div>

Note that DGM will automatically determine if the simulation is 2D or 3D, so only one of the numbers of electrodes (1000 in 3D, 29x29 in 2D) will be used.
To convert the mesh from the meshalyzer files to a vtk file, one can use the following command:

<div align="center">$ meshtool convert -omsh=block -imsh=block -ofmt=vtk -ifmt=carp_txt</div>

As loading this file can take a while, DGM also provides a *LAT_p.txt* file after a first analysis. This file can be immediately loaded in the GUI for further analysis to speed up the computations.

3.1.4 PPI-TCL, ablation points and corresponding tags

In case the study's xml is uploaded for a CARTO file and the predefined tags as presented in table 3 were used during the procedure to label certain electrodes, one can visualize not only the analysis of DGM but as well PPI-TCL locations with corresponding colors. Scar regions, double potentials and fragmented signals can be annotated during the procedure on the CARTO module and visualized in DGM in case the tags are used correctly.

In case one uses RHYTHMIA, the spatial location of your ablation points are needed and a calculation editor such as Excel will be necessary to create the template PPI file. For simulations, one can use the same template format. The basic format should contain the XYZ coordinates and the color label of the PPI-TCL point. Default options are: "green", "yellow", "red", "blue", "black", "white", "orange", "purple", "pink" and "grey". One can also use DGM to visualize the arrhythmia with additional nodes providing useful information or to tag certain regions.

The following table provides possible tags which can be used in the file.

tag	meaning	color in DGM
SCAR	indication of scarred regions	grey
POTENTIAL	indication of double potentials	blue
SIGNAL	fragmented signal	pink
30	PPI-TCL < 30 ms	green
50	PPI-TCL < 50 ms	yellow
BAD	PPI-TCL > 50 ms	black

Table 3: **Automatically visualized CARTO tags** In case during the procedure a specific electrode recordings is labeled with the tags presented in the tag-column, DGM will automatically find them in the .xml file and visualize them with corresponding colors in the GUI.

The following format can be used to show the PPI-TCL points in DGM:

x,	y,	z,	color
x0,	y0,	z0,	color0
x1,	y1,	z1,	color1
x2,	y2,	z2,	color2
...			

Table 4: **PPI-TCL template format.** A comma-separated file will enable a user to visualize the PPI-TCL points or other desired tags and points, such as annotated scar, denoted slow conductive channels, indicated double potentials or ablation targets. Again, the top line should be omitted.

3.2 Output generated by DGM

Once the input files are generated or extracted from a mapping system, a simulation or an experimental set-up, one can process the data with DGM by opening the GUI. Once loaded into the software, by pressing calculate, DGM will automatically search for rotational and/or focal activity present in the data.

For further processing of the data generated by DGM, we will give an overview of the output which is generated by DGM. First, in the main folder, a *period.json* file is generated which stores the period of the arrhythmia. In case the arrhythmia is irregular, this is also stored in this file. All the other output files are generated in a separate folder in the main data folder called "output". These files are generated by the core algorithm, which are used for the visualization of the results. Of course, one can also use the files in the output folder for a different visualization tool. Note that most files have either the time of calculation and/or number of nodes in the filename. For example *result_loops_t0.csv* contains all the accepted loops found at 0 ms. The following output files are generated:

- **result_loops_t{time}.csv**

  x_core, y_core, z_core, amount, variance, intervariability, length, index0, LAT0, index1, LAT1, ...

  Each row of this files provides detailed information about the different reentry cycles which are visualized in the GUI. The first 3 columns correspond with the location of core of the reentry loop. *Amount* is a measure for the number of different cycles which are detected by DGM and belong to the same reentry loop. *Variance* is a measure for the uniformity of the reentry, see also section 2.2. *Intervariability* is the absolute value of the maximal deviation of the LATs from the straight line used to calculate the variance. *Length* is the accumulative length of the reentry by taking the sum of the euclidean distances between the nodes. Next follows a series of indices and their corresponding LATs which belong to the chosen cycle. Each electrode or node has a unique index.

- **result_focal_t{time}.csv**

  x_core, y_core, z_core, amount, variance, intervariability, length, index0, LAT0, index1, LAT1

  Each row determines represents an arrow which contributes to the visualization of the focal beats. For easy implementation, we copied the same format as the loops. However, only index0 and index1 are used as each row represents a directed arrow from index0 to index1.

- **front_t{time}_p{nodes}.csv**

$$\text{color,} \quad \text{scalar,} \quad \text{x,} \quad \text{y,} \quad \text{z,} \quad \text{x\_dir,} \quad \text{y\_dir,} \quad \text{z\_dir}$$

Each row in this file represents a single arrow of our wavefront. The wavefront is a collection of arrows which gives a visual representation of the electrical flow. *Color* represents a time associated to the arrow which is a value larger than the time t upon the directed network is created. *Scalar* is the normalized size of the arrow and should always be one. (x, y, z) is the 3D spatial location of the starting point of the arrow whilst (x_dir, y_dir, z_dir) is the normalized direction of the wave arrow. Drawing all these arrows creates a wavefront generated by DGM.

- **loopband_t{time}_p{nodes}.csv**

$$\text{color,} \quad \text{scalar,} \quad \text{x,} \quad \text{y,} \quad \text{z,} \quad \text{x\_dir,} \quad \text{y\_dir,} \quad \text{z\_dir}$$

Each row in this file represents an arrow in the loopband in the same format as the previously described wavefront. The loopband creates an easy-to-interpret visualization of a region around the detected loops.

- **mesh_t0_p0.csv**

$$
\begin{array}{ccc}
\text{x,} & \text{y,} & \text{z} \\
\text{x0,} & \text{y0,} & \text{z0} \\
\text{x1,} & \text{y1,} & \text{z1}
\end{array}
$$

This file represents the mesh which was used for the visualization, which can also be used in other visualization tools (e.g. Paraview). It contains the spatial coordinates of the mesh nodes. The top line is also included in the mesh file.

3.3   Visualization

DGM has two layouts, the basic view and the advanced view. Depending on your default setting, the application will open in either the basic or the advanced view.
The basic view allows little room for adaptions and is ideal for a first use of DGM. The advanced layout allows the user to change many parameters of the program. We will explain in detail all the possibilities of both layouts.

3.3.1   Basic layout

In our basic layout (see Figure 3), only a very limited set of options are available to process the input data. First, one needs to chose the input file. This can be done by pressing the button 'select file' in the setting Window (see Figure) and navigating in the pop-up to the folder which contains the data of interest. We recommend to put each case in a separate folder. If the data contains a single LAT for each node, the user has to fill in the cycle length of the arrhythmia (regular case). This field is blocked when more than one LAT is given per node (irregular case). The interval sets the different times that DGM processes the data. For regular cases, the start is automatically set to 0 ms, the end to the cycle length and the interval to 5 ms. For irregular cases, the start is set to the largest LAT of the first column of each node and the end is set to the smallest LAT of the last column of each node. The step size is set to 20 ms. All these values can be changed upon user preference. For example, if the calculations are too lengthy, one can opt to increase the step size.
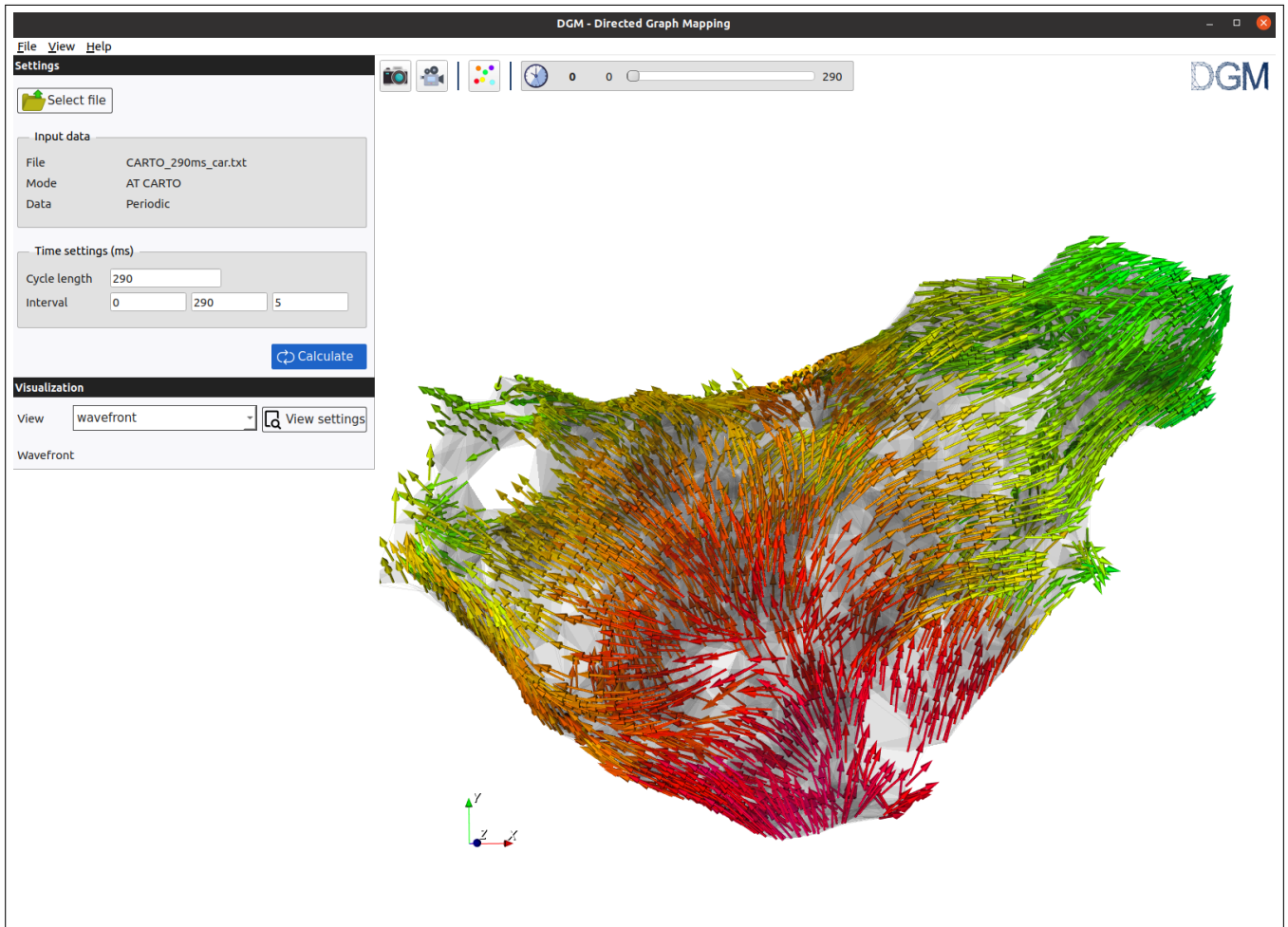
Figure 3: **Basic layout**

Next, the user has to press the 'Calculate' button. As a result, DGM will search for closed loops in the network and focal sources. To visualize the results, the user can chose between the following preset view templates:

> **loops** this template shows the reentry loops with the lowest variance
>
> **focal** this template shows the focal sources
>
> **loopband** this template gives a clear view of the reentry cycles by adding a band of arrows
>
> **wavefront** visualization of the wave propagation

For CARTO cases, if the appropriate files are exported, PPI-TCL and ablation can also be shown.

> **ablation** in this template the user can check if the ablation target indeed cuts the loopband
>
> **ppi** this template will show the measured ppi points
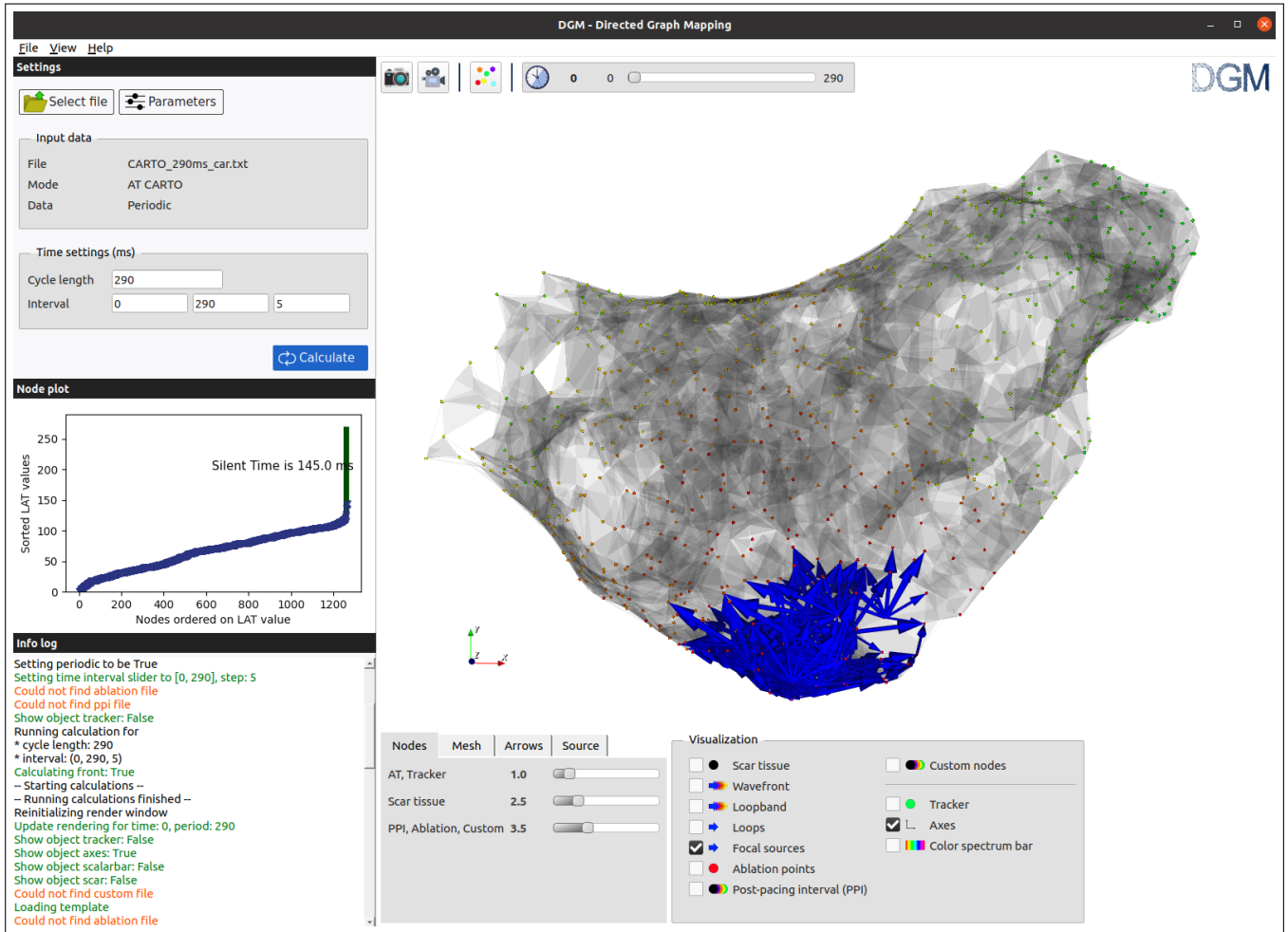
3.3.2 Advanced layout

Figure 4: **Advanced view**

In the advanced layout (see Figure 4), many more options are available to process the data. In this section, we will give an overview of the additional features of this layout. The selection and calculations follow the same process as in the basic layout.

Settings - parameters
In the advanced layout, the user can change the settings of the search algorithm for finding cycles in the network. Only when you load a general data file, all settings can be changed. For the company mapping datasets, the user cannot alter any parameters as they are currently hard coded in the software.

Minimal arrow count	One can choose the minimal necessary arrows which should be present in a cycle. Standard this is set to 9, but it can be necessary to lower this number for sparse datasets.
Variance	This measure, previously called "phase variance", was described in Van Nieuwenhuyse et al. [68] and in section 2.2.
Intervariability	The intervariability was explained in section 3.2.
Distance (mm)	The maximum allowed distance between two neighbours. If the Euclidean distance between two nodes is larger than this value, DGM does not allow them to be neighbours.
Focal threshold	The period will be divided by this number resulting in an amount of bins for which we will cluster the network, see section 2.3. In case irregular data is presented, the period is calculated as the average period based on the first two LATs after the considered time t.
Cvmin (mm/ms)	The minimal allowed conduction velocity used for the construction of the directed graphs as explained in section 2.
Cvmax (mm/ms)	The maximal allowed conduction velocity used for construction of the directed graphs as explained in section 2.
Merge jump	This is the value δt which connects the two different graphs which will be merged to the final graph as explained in section 2.
Core separator (mm)	This value represents the core separation in mm. This means that if the center of two cycles lies closer than this value, the cycle with the lowest variance will be chosen. In case the core of two cycles is larger than this value, they will be displayed individually.

Node plot

The node plot works for regular arrhythmia and shows the nodes ordered according to the LAT value on the x-axis, and their corresponding LAT values on the Y-axis, see Figure 5. This is especially useful for atrial tachycardia or ventricular tachycardia as this is an indication of the reentry mechanism: focal in case of a large silence time; reentrant in case of a small or no silence time. We note that this differs, albeit slightly, from the global cycle length coverage previously described [72]. However, in Vandersickel et al. [69], our group also introduced the concept of silent time as the time between the last activation (LAT of a node) of a beat and the first activation (LAT of another node) of the next beat. However the correlation between the silent time and the mechanism of the arrhythmia is not bulletproof. Therefore, DGM looks for both focal activity as well as reentries, as setting an automatic threshold on the silent time to differentiate between reentry and focal activity could exclude some marginal cases.
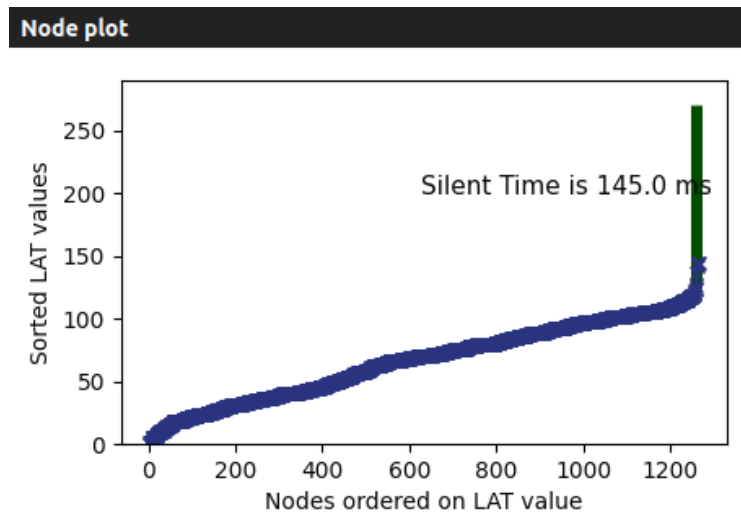
Figure 5: **LAT node plot**

Info log
The info log shows the internal output of the program. This can be useful to find why certain visualizations do not work and can give valuable feedback in case something does not work in the program. Under *File → Settings* in the top menu the user can change the default logging level.

Visualizations
The advanced mode allows to change most aspects of the visualization in the following part of the GUI:
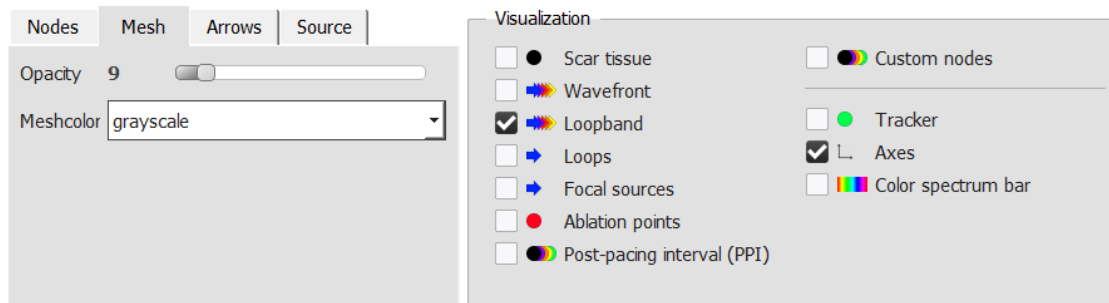

Figure 6: **Rendering options**

The first left box contains several tabs to alter specific settings:

Mesh   Change color and opacity of the mesh

Nodes   Change size of different nodes

Arrows   Change size and color scheme of arrows

Source   Change the allowed variance of displayed loops. The more the slider is set to the right, the more the variance is lowered. Therefore, less loops will be displayed, but with higher confidence.

The second and third box allows the user to select in detail what needs to be visualized. The icons show whether the visualization is a node or an arrow and whether it has a single fixed color or a range of colors.

3.3.3 Icon bar

In both views, using the icons in the top bar, the user has the option to make either a screenshot of their rendering or a movie of the given time interval. Furthermore there is the option to load a custom node file which can be added to the rendering.

Figure 7: **Icon bar**

(1) Create image	Create an image of the current rendering.
(2) Create video	Create a video of the rendering over the set time interval in either *.ogg* of *.mp*4 format.
(3) Custom nodes	Load your own custom nodes file to add to the rendering.
(4) Time interval	For irregular arrhythmia, the time slider allows the user to go forward in time and analyze the arrhythmia for the different time intervals as entered in the settings before pressing calculate. For a regular arrhythmia, the interval will be set between 0 and the cycle length for a more dynamical view of the arrhythmia.

3.3.4 General settings

In the top menu of the program, the user can chose some additional settings:

- File: General application settings:
  - **File selection on startup**: the user can chose that a pop-up opens upon start for the file selection
  - **Advanced layout**: the user can select if the program will open in the advanced lay-out
  - **Clear output**: if this option is chosen, the output will be cleared upon closing the program/opening a certain file
  - **Debug logging**: a choice between the default info messages or additional in depth debugging output as well
- View: The following views can be chosen
  - **Advanced layout**: this lets you chose between the advanced or the basic layout
- Help: provides the link to the documentation of DGM and to the academic licence of DGM.
  - **Documentation**: link to the documentation section of the DGM website.
  - **About DGM**: General application info such as version number, as well as a link to the software licence.

4 Some basic examples

In this section we will discuss all the possible combinations of input that the program can handle. This can be useful for the user to experiment with DGM and to create its own input files. These files can be downloaded from our site and should be bug free.

The first example presented is a **regular simulation with reentry in 3D**, corresponding to frame A in Figure 8. To create this Figure, the user should load *LAT_p*2000.*txt*. The mesh presented in panel A1 will be generated. After pressing Calculate, the outcome in A.2, A.3 and A.4 will be shown either clicking the wavefront, loops or loopband button. In Supplementary Movie 1, an animated loopband is presented. As a second example, we show a **regular simulation with focal activity in 2D** starting from the lower left. Panel B.1 shows the original selected electrodes, while panel B.2 and B.3 present the results after calculation. In Supplementary Movie 2, we show the animated wavefront for a single focal beat. The third example is a **irregular simulation with reentry in 2D**. After processing the data, in panel C.1 one observes the electrodes including scar tissue. In panel C.2, we shown the wavefront, panel C.3 shows the reentry cycles which show anatomical reentry around the right scar tissue, and in panel C.4 we show the loopband. Additionally, one can download the corresponding *ppi.txt* file online and load it as a custom file. This file shows the simulated PPI-TCL measurements on the location

indicated in panel C.5. Supplementary Movie 3 summarized the results of this case. In panel D, we present **an irregular simulation with focal activity in 3D**. The same case is also illustrated in Supplementary Movie 4.
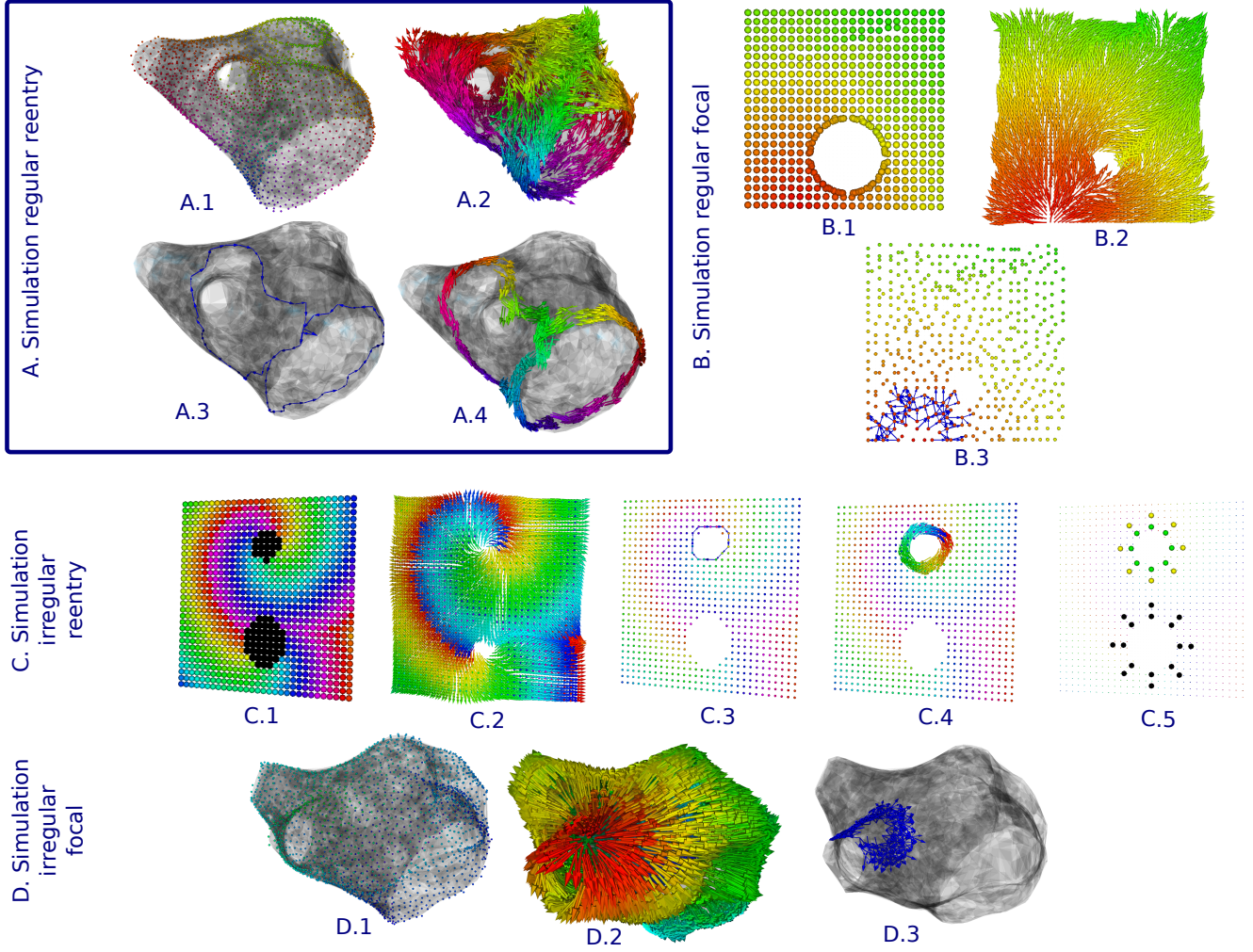

Figure 8: 4 simulated examples, see text for explanation.

In panel E, we show a **Regular reentry recorded by CARTO**. Moreover, this is a double loop AT: one macro reentry around the mitral valve and one localized reentry at the anterior wall around some scar tissue. In panel F, we show a **regular focal recorded by CARTO**. To be more specific, this is actually a breakthrough from a right sided AT. As discussed before, the inital electrode positions of CARTO (E.1 and F.1) are redistributed (E.2 and F.2). Based on this new nodes, DGM calculated a wavefront (E.3 and F.3) and in case of reentry, displays the loopband (E.4). In case you have a focal arrhythmia, you will have to switch to the focal button (F.4). Also illustrated in panel E.5 are the PPI-TCL recordings from the *.xml* file and the ablation sites found in the $VisiTagExport/Sites.txt$ file. We also present two additional supplementary movies, Supplementary Movie 5 and Supplementary Movie 6, which show the loopband of the reentry case E and the wavefront of the focal breakthrough F. For privacy reasons, we have created our own CARTO files, which are no longer linked to a certain patient.
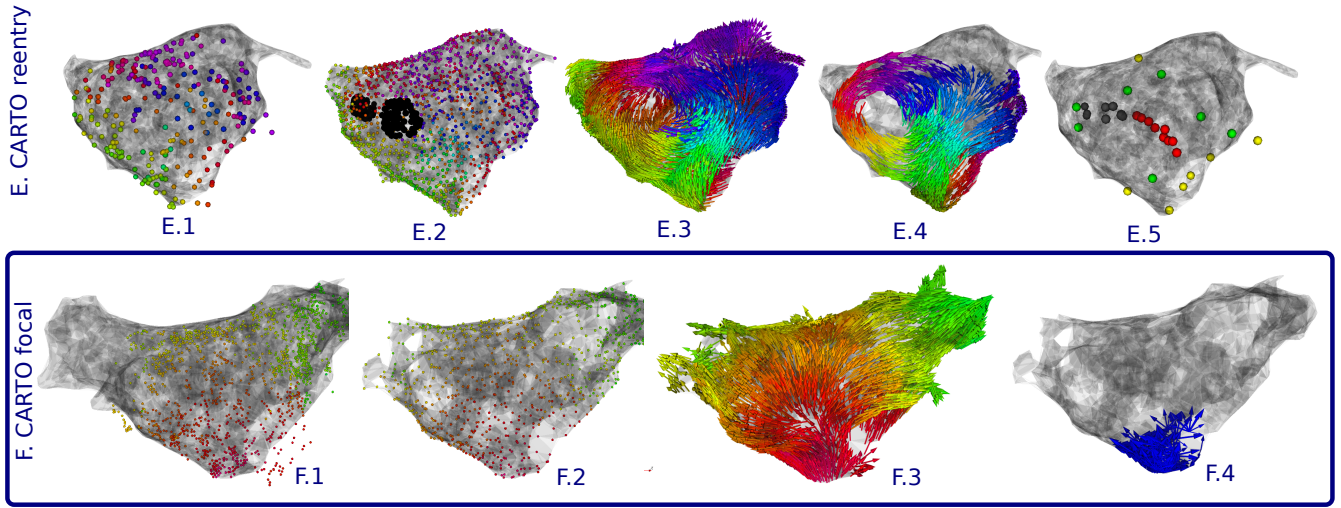
Figure 9

Finally, we also show one example of a **irregular reentry in 3D simulated by openCARP**. To render these pictures, one has to load the openCARP *.igb* file. DGM will create the standard *LAT_p.txt* file. In panel G.1 the nodes are shown, in panel G.2 the loopband is presented, in panel G.3 the wavefront is shown, and in panel G.4 the cycles are plotted.
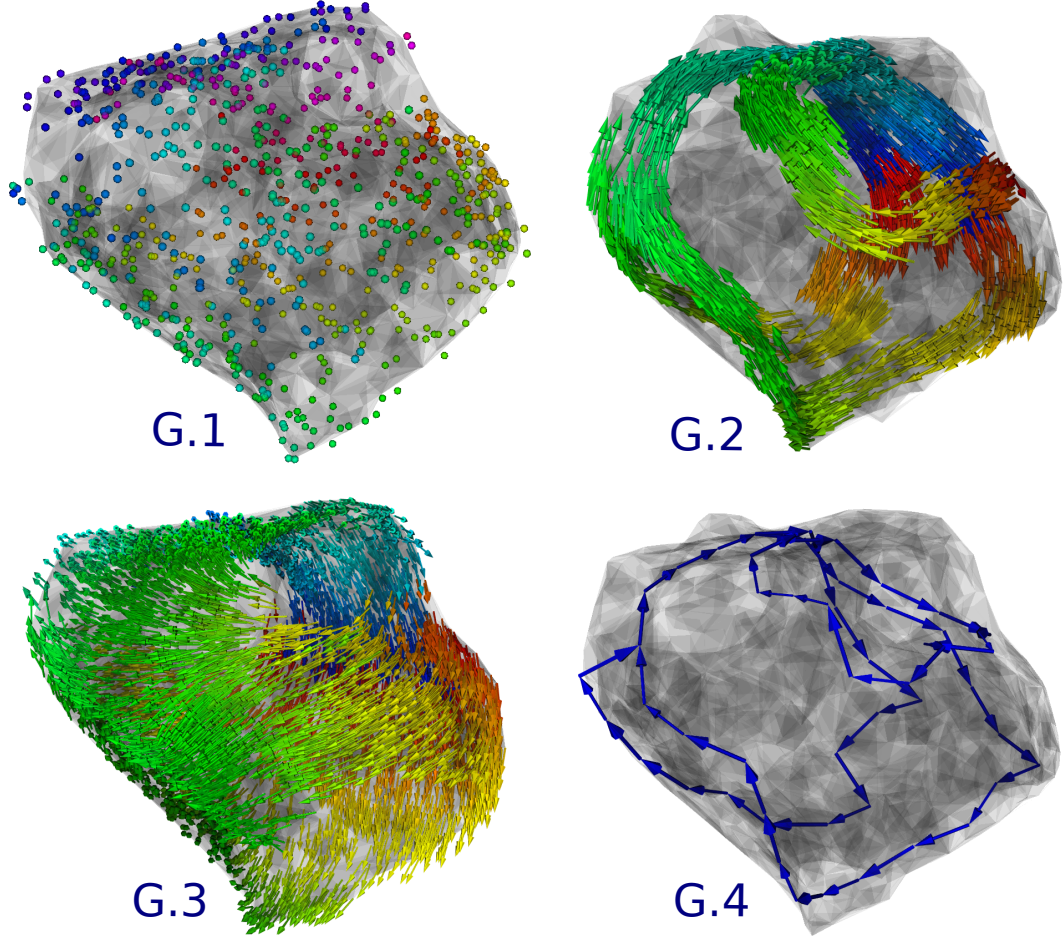
Figure 10

5 Summary of the data which is already processed by DGM

In this section, we give an overview of the type of datasets which were already processed with DGM. We divide this section according to the type of arrhythmia.

5.1 Atrial tachycardia - AT

DGM has been mainly optimized to work with data from AT. In a first study [44], we compared the ablation target of 31 cases of AT which would be chosen based on DGM with the actual ablation target and DGM had a 100% success rate. In a second study, 51 complex ATs were retrospectively analyzed with DGM, whereby entrainment mapping determined the actual reentry loop in case of reentry [68]. Experts diagnosed the correct AT mechanism and location with the latest mapping software of CARTO in 33 cases versus DGM in 38 cases. Even though a lot of thought went into these cases, we explicitly note that this was a single centered study. Hence we except that the automated performance will first drop and a modification of the now fixed parameters might be required to further develop and improve DGM.

So far all published data was on cases of Biosense Webster, although DGM can also work with the RHYTHMIA (Boston Scientific) system. Upon loading a *.mat* file, this data is processed and gives a result based on the analysis of a single center as well. However, no entrainment study on RHYTHMIA data is yet available to us, to know the ground truth. In the future, we aim to analyze and optimize DGM based on EM guided ablations of AT with the aid of RHYTHMIA electrode recordings.

5.2 Atrial fibrillation - AF

So far, we only analyzed simulated basket catheter data of a meandering spiral wave in the right atrium, causing the left and right atrium to fibrillate. It has been reported that upon analysis with PM, wrong rotors emerged due to the interpolation artefacts and the far field, obstructing correct interpretation of the single meandering rotor [45]. By changing the minimal conduction velocity in DGM, we were able to differentiate the false rotors from the true rotor [70], overcoming some of the artefacts of PM.

5.3 Torsade de Pointes - TdP

DGM was originally developed to analyze needle data of chronic atrioventricular block (CAVB) dog model, known for its high susceptibility for of Torsade de Pointes (TdP). TdP is a dangerous arrhythmia, as it can degenerate into ventricular fibrillation and cause sudden cardiac death also in children en young adults [73]. Although TdP is such an important arrhythmia, still many aspects of the mechanism remain unclear. Many studies agree that a TdP starts with a focal beat which is caused by a group a cells experiencing an early after depolarizations (EAD) at the same time [74, 75, 76, 77, 78, 79, 80, 81]. However, contrary to the established mechanism of the trigger of TdP, the perpetuation of TdP remains controversial. Focal mechanisms [79, 81, 75, 80, 82, 83, 84], non-stationary reentries [77, 78, 85] or both mechanisms [74, 76, 82] were claimed to underlie to basis of the perpetuation of a TdP. With an early version of DGM, we analyzed 54 episodes of TdP in 5 susceptible dogs and found that TdP can be driven by focal activity as well as by re-entry depending on the duration of the episode. Short lasting episodes were maintained by focal sources, while longer lasting and non-terminating episodes were maintained by reentry [69]. With the latest version of DGM, we are currently further characterizing the types and numbers of reentry during the longer lasting episodes.

5.4 Simulations to compare DGM with PM

DGM could be a useful tool in comparison with PM, as we have previously shown that DGM is more robust compared to PM in case noise is added to the LATs [44]. In this paper, we simulated a single rotor which we measured with 256 evenly distributed electrodes. We added Gaussian noise to the LATs, which were derived as the steepest derivatives on the measured signals. We then compared the performance of DGM with PM, and found that for 20 ms of Gaussian noise, DGM was still 80% effective, while PM was unable to detect the single rotor correctly (0%). Instead of a single diagnosis, PM either did not found the center rotor or found the center rotor in addition with multiple other sites showing rotational activation.

The reason why phase-mapping fails in this in-silico setting is twofold. First, PM easily detect false positives. The basic concept of PM is to search for a 2π enclosure around a line integral created by neighboring electrodes. Usually only four electrodes are taken into account. A single alteration of a LAT can therefore result in a misplaced detection. For the same reason, as only four neighbours are taken into account to find the true phase singularity, a mistake in one of these four neighbours can result in a false negative. As DGM is a global measure, it overcomes this shortcoming of the local PM.

However, a more profound analysis of DGM versus PM is necessary as we used a single implementation of PM based on the LATs. More on this in the Discussion section of this manuscript.

5.5 Future studies

We are currently also processing data of hemodynamical stable **VTs**, which were recorded by CARTO in a sequential way. We found that we can analyze these datasets in a very similar way as the ATs, however, we do need to adapt our parameters to optimize the analysis of DGM. Next, we are also analyzing extremely rare socket data of episodes of **VF** to better understand the mechanism of VF. We are currently comparing our results with previously performed analysis of PM. We aim to visualize the excitation fronts of the arrhythmia with the wavefront feature of DGM. We stress again that due to the generality of DGM, there is no limit to the type of dataset DGM can analyze, although each dataset will require specialized additional algorithms to optimize the analysis.

6   Discussion

6.1   DGM as a tool to process arrhythmia: moving forward to a clinical application

This manuscript presents the first version of DGM, a software package to automatically analyze any given dataset of an arrhythmia. The minimal input of this software is a single datafile containing the LATs and corresponding spatial distribution of the electrodes which were used to measure the arrhythmia under study. DGM can work with regular arrhythmia (a single LAT per coordinate) or irregular arrhythmia (multiple LATs per coordinate). DGM processes the data by creating a directed network of the excitation of the arrhythmia. In short, rotational activity is found by detected the cycles in the network and focal activity by detecting regions with only outgoing arrows. By making the program public for academic use, we hope to contribute to the community by making the analysis of arrhythmia fast and robust.

One of the major problems in science is reproducability of results. For DGM to be a reliable tool which could eventually be used for ablation procedures, it has to be validated on many different datasets, different systems and different hospitals. It is therefore of paramount importance that DGM will be further validated by different EPs in different hospitals. Moreover, based on new input, DGM needs to be further optimized. Our final goal would be to integrate DGM in an (multiple) existing mapping system(s) if it can be proven that DGM makes the procedures faster and more robust. AT is currently the most developed application of DGM, but we hope to show that DGM is also useful for other arrhythmias.

Another major problem is access to novel data. Due to privacy reasons, data sharing always needs consent of the patient, which can be difficult to obtain afterwards. We therefore recommend that EPs ask consent of the patient before the procedure, for data to be processed afterwards.

6.2   Choosing the right parameters for optimal clinical outcome

DGM is currently manually and empirically optimized to find the best outcome based on datasets from a single centre (AZ Sint Jan Bruges). We realize that smarter and more advanced tools are available to find an optimal parameter setting (such as genetic evolution and neural networks approaches). However, we need to collect huge amounts of data, from which we know the ground truth before we can automatically optimize DGM. For example, to automatically optimize AT we need a large cohort of data including a careful entrainment mapping study for each case.

6.3   LAT annotation: which annotation to use?

Currently, we completely rely on CARTO and RHYTHMIA annotated LAT for the analysis of DGM in clinical settings. However, we are currently working on implementing our own annotation for regular arrhythmia, which gives a similar outcomes as using the company annotations.

For irregular arrhythmia, like AF, annotations can be tedious [86] to impossible. Therefore, one of our future goals is to make DGM independent of the LAT annotation and draw arrows based on the ECGM signals of two neighboring electrodes and their causal correlations.

6.4   Interpolation

DGM is currently not able to interpolate signals on unmapped regions. Therefore, DGM does not analyze regions where no electrode recordings are taken. Hence, it is key to have a uniform distribution of the spatial electrodes. The interpretation of the arrhythmia will not be accurate in case e.g. solely the anterior wall is mapped.

6.5   Optimal amount of electrodes

Not only the uniformity but also the total amount of electrodes play an important role with respect to the scale of the arrhythmia. One can appreciate that if little electrode recordings are taken while also some electrode recordings are inaccurately annotated, the LAT-representation can differ significantly from the ground truth. We have noticed that this plays in important role in the common isthmus of a double loop circuit.

Therefore, in case of a regular AT, DGM needs around 500 to 1500 points which are uniformly distributed. However, the software can also handle ATs with a density of around 200 points, but this might lead to wrong diagnosis certainly in cases where wrongly annotated signals tend to play a keyrole in the interpretation of the AT. Changing a single electrode recording in a sparse network can have a big influence, while DGM would be

able to discard this electrode if the network was more dense. If is of course logical that in case solely the anterior wall is mapped and the reentry or focal breaktrough/automaticity is located at the posterior wall, DGM will not be able to diagnose the AT.

On the other hand, in case you have an abundance amount of electrode recordings (such as over 3500), DGM will reduce this amount in a smart way. This is because the BFS algorithm slows down when more points are added. Also, we noticed that for regular ATs, having more than 20 points at the same 1 cm^2 is not necessary as there is enough information in these 20 points.

In conclusion, we advise to have at least 500 uniformly distributed points in the atrium to record a regular AT. We do realize this is not always possible in unstable arrhythmias. Moreover, for VT, it might not be possible as the arrhythmia is not hemodynamically stable. To overcome this issues, we will have to look for additional algorithms, which can also analyze sparse data, or partial datasets.

6.6   DGM and PM

As PM remains one of the most popular methods to analyze cardiac data, we also plan to implement PM methods so the user can compare DGM with PM. This can save time for researchers which want to implement PM while also enabling a more standardized approach for PM guided research.

In addition, we have already implemented a hybrid approach combining DGM with PM (which we will be released in the future). In this approach the velocity restriction to construct the network is eliminated, while the locality of PM is globalized. It gives the possibility to give a likelihood on the detection by PM by means of the variance and intervariability, in contrast with the discrete yes/no outcome of PM. So in complex data annotation were choosing a velocity is not desired, this hybrid method could be a solution. Moreover, this would allow us to use a Hilbert transform as presented in [37], overcoming the previously mentioned problems of annotating the LATs.

Supplementary Material

Supplementary Movie 1 - Simulation Regular Reentry

https://www.dropbox.com/s/lnygpew7fqlvn6r/SupplementaryMovie1.mp4?dl=0

Supplementary Movie 2 - Simulation Regular Focal

https://www.dropbox.com/s/5ogaesmu0i5p5xf/SupplementaryMovie2.mp4?dl=0

Supplementary Movie 3 - Simulation Irregular Reentry

https://www.dropbox.com/s/xh1wvfhcruze9ht/SupplementaryMovie3.mp4?dl=0

Supplementary Movie 4 - Simulation Irregular Focal

https://www.dropbox.com/s/0stwhjsy9u53qfr/SupplementaryMovie5.mp4?dl=0

Supplementary Movie 5 - CARTO Regular Reentry

https://www.dropbox.com/s/w5cp55xxa17y3c4/SupplementaryMovie6.mp4?dl=0

Supplementary Movie 6 - CARTO Regular Focal

https://www.dropbox.com/s/fx4vdt5x2wvoj2h/SupplementaryMovie7.mp4?dl=0

References

[1] Douglas N Gibson, Luigi Di Biase, Prasant Mohanty, Jigar D Patel, Rong Bai, Javier Sanchez, J David Burkhardt, J Thomas Heywood, Allen D Johnson, David S Rubenson, et al. Stiff left atrial syndrome after catheter ablation for atrial fibrillation: clinical characterization, prevalence, and predictors. *Heart Rhythm*, 8(9):1364–1371, 2011.

[2] Steven M Pogwizd, RH Hoyt, JE Saffitz, PB Corr, James Lewis Cox, and ME Cain. Reentrant and focal mechanisms underlying ventricular tachycardia in the human heart. *Circulation*, 86(6):1872–1887, 1992.

[3] Teresa Strisciuglio, Nele Vandersickel, Giuseppe Lorenzo, Enid Van Nieuwenhuyse, Milad El Haddad, Jan De Pooter, Maria Kyriakopoulou, Alexandre Almorad, Michelle Lycke, Yves Vandekerckhove, et al. Prospective evaluation of entrainment mapping as an adjunct to new-generation high-density activation mapping systems of left atrial tachycardias. *Heart rhythm*, 17(2):211–219, 2020.

[4] Milad El Haddad, Richard Houben, Rene Tavernier, and Mattias Duytschaever. Stable reentrant circuit with spiral wave activation driving atrial tachycardia. *Heart Rhythm*, 11(4):716–718, 2014.

[5] Michel Haissaguerre, Pierre Jaïs, Dipen C Shah, Atsushi Takahashi, Mélèze Hocini, Gilles Quiniou, Stéphane Garrigue, Alain Le Mouroux, Philippe Le Métayer, and Jacques Clémenty. Spontaneous initiation of atrial fibrillation by ectopic beats originating in the pulmonary veins. *New England Journal of Medicine*, 339(10):659–666, 1998.

[6] Anthony G Brooks, Martin K Stiles, Julien Laborderie, Dennis H Lau, Pawel Kuklik, Nicholas J Shipp, Li-Fern Hsu, and Prashanthan Sanders. Outcomes of long-standing persistent atrial fibrillation ablation: a systematic review. *Heart Rhythm*, 7(6):835–846, 2010.

[7] R Weerasooriya, P Khairy, J Litalien, L Macle, et al. Catheter ablation for atrial fibrillation: are results maintained at 5 years of follow-up? jacc 2011; 57: 160-166. 21. altman rk, proietti r, barett cd, perini ap et al. management of refractory atrial fibrillation post surgical ablation. *Ann Cardiothorac Surg*, 3(1):91–97, 2014.

[8] James N Weiss, Zhilin Qu, and Kalyanam Shivkumar. Ablating atrial fibrillation: A translational science perspective for clinicians. *Heart rhythm*, 13:1868–1877, Sep 2016.

[9] Caroline H Roney, Andrew L Wit, and Nicholas S Peters. Challenges associated with interpreting mechanisms of af. *Arrhythmia & Electrophysiology Review*, 8(4):273, 2020.

[10] Gordon K Moe, Werner C Rheinboldt, and JA Abildskov. A computer model of atrial fibrillation. *American heart journal*, 67(2):200–220, 1964.

[11] Maurits A Allessie. Experimental evaluation of moe's multiple wavelet hypothesis of atrial fibrillation. *Cardiac electrophysiology and arrhythmias*, pages 265–275, 1985.

[12] Phillip S Cuculich, Yong Wang, Bruce D Lindsay, Mitchell N Faddis, Richard B Schuessler, Ralph J Damiano Jr, Li Li, and Yoram Rudy. Noninvasive characterization of epicardial activation in humans with diverse atrial fibrillation patterns. *Circulation*, 122(14):1364–1372, 2010.

[13] Nicholas Child, Richard H Clayton, Caroline R Roney, Jacob I Laughner, Allan Shuros, Petr Neuzil, Jan Petru, Tom Jackson, Bradley Porter, Julian Bostock, et al. Unraveling the underlying arrhythmia mechanism in persistent atrial fibrillation: results from the starlight study. *Circulation: Arrhythmia and Electrophysiology*, 11(6):e005897, 2018.

[14] R. H. Keldermann, K H W J. ten Tusscher, M. P. Nash, C. P. Bradley, R. Hren, P. Taggart, and A. V. Panfilov. A computational study of mother rotor vf in the human ventricles. *Am J Physiol Heart Circ Physiol*, 296(2):H370–H379, Feb 2009.

[15] José Jalife, Omer Berenfeld, and Moussa Mansour. Mother rotors and fibrillatory conduction: a mechanism of atrial fibrillation. *Cardiovascular research*, 54(2):204–216, 2002.

[16] Sanjiv M. Narayan, David E. Krummen, Kalyanam Shivkumar, Paul Clopton, Wouter-Jan Rappel, and John M. Miller. Treatment of atrial fibrillation by the ablation of localized sources: Confirm (conventional ablation for atrial fibrillation with or without focal impulse and rotor modulation) trial. *Journal of the American College of Cardiology*, 60(7):628–636, Aug 2012.

[17] Sanjiv M Narayan, Tina Baykaner, Paul Clopton, Amir Schricker, Gautam G Lalani, David E Krummen, Kalyanam Shivkumar, and John M Miller. Ablation of rotor and focal sources reduces late recurrence of atrial fibrillation compared with trigger ablation alone: extended follow-up of the confirm trial (conventional ablation for atrial fibrillation with or without focal impulse and rotor modulation). *Journal of the American College of Cardiology*, 63:1761–1768, May 2014.

[18] Ross Morgan, Michael A Colman, Henry Chubb, Gunnar Seemann, and Oleg V Aslanidi. Slow conduction in the border zones of patchy fibrosis stabilizes the drivers for atrial fibrillation: insights from multi-scale human atrial modeling. *Frontiers in physiology*, 7:474, 2016.

[19] Edward Vigmond, Ali Pashaei, Sana Amraoui, Hubert Cochet, and Michel Hassaguerre. Percolation as a mechanism to explain atrial fractionated electrograms and reentry in a fibrosis model based on imaging data. *Heart Rhythm*, Mar 2016.

[20] Michel Haissaguerre, Meleze Hocini, Arnaud Denis, Ashok J Shah, Yuki Komatsu, Seigo Yamashita, Matthew Daly, Sana Amraoui, Stephan Zellerhoff, Marie-Quitterie Picat, et al. Driver domains in persistent atrial fibrillation. *Circulation*, 130(7):530–538, 2014.

[21] Jason D Bayer, Caroline H Roney, Ali Pashaei, Pierre Jaïs, and Edward J Vigmond. Novel radiofrequency ablation strategies for terminating atrial fibrillation in the left atrium: a simulation study. *Frontiers in physiology*, 7:108, 2016.

[22] Sohail Zahid, Hubert Cochet, Patrick M. Boyle, Erica L. Schwarz, Kaitlyn N. Whyte, Edward J. Vigmond, Rémi Dubois, Mélèze Hocini, Michel Haïssaguerre, Pierre Jaïs, and Natalia A. Trayanova. Patient-derived models link reentrant driver localization in atrial fibrillation to fibrosis spatial pattern. *Cardiovasc Res*, Apr 2016.

[23] Maurits A Allessie, Natasja MS de Groot, Richard PM Houben, Ulrich Schotten, Eric Boersma, Joep L Smeets, and Harry J Crijns. Electropathological substrate of long-standing persistent atrial fibrillation in patients with structural heart diseaseclinical perspective. *Circulation: Arrhythmia and Electrophysiology*, 3(6):606–615, 2010.

[24] Natasja de Groot, Lisette Van Der Does, Ameeta Yaksh, Eva Lanters, Christophe Teuwen, Paul Knops, Pieter van de Woestijne, Jos Bekkers, Charles Kik, Ad Bogers, et al. Direct proof of endo-epicardial asynchrony of the atrial wall during atrial fibrillation in humans. *Circulation: Arrhythmia and Electrophysiology*, 9(5):e003648, 2016.

[25] Natasja MS de Groot, Richard PM Houben, Joep L Smeets, Eric Boersma, Ulrich Schotten, Martin J Schalij, Harry Crijns, and Maurits A Allessie. Electropathological substrate of longstanding persistent atrial fibrillation in patients with structural heart diseaseclinical perspective. *Circulation*, 122(17):1674–1682, 2010.

[26] Ali Gharaviri, Simone Pezzuto, Mark Potse, Sander Verheule, Giulio Conte, Rolf Krause, Ulrich Schotten, and Angelo Auricchio. Left atrial appendage electrical isolation reduces atrial fibrillation recurrences: A simulation study. *Circulation: Arrhythmia and Electrophysiology*, pages CIRCEP–120, 2020.

[27] Brian J Hansen, Jichao Zhao, Thomas A Csepe, Brandon T Moore, Ning Li, Laura A Jayne, Anuradha Kalyanasundaram, Praise Lim, Anna Bratasz, Kimerly A Powell, et al. Atrial fibrillation driven by micro-anatomic intramural re-entry revealed by simultaneous sub-epicardial and sub-endocardial optical mapping in explanted human hearts. *European heart journal*, 36(35):2390–2401, 2015.

[28] Jichao Zhao, Brian J Hansen, Yufeng Wang, Thomas A Csepe, Lidiya V Sul, Alan Tang, Yiming Yuan, Ning Li, Anna Bratasz, Kimerly A Powell, et al. Three-dimensional integrated functional, structural, and computational mapping to define the structural "fingerprints" of heart-specific atrial fibrillation drivers in human heart ex vivo. *Journal of the American Heart Association*, 6(8):e005922, 2017.

[29] David E Krummen, Gordon Ho, Christopher T Villongco, Justin Hayase, and Amir A Schricker. Ventricular fibrillation: triggers, mechanisms and therapies. *Future cardiology*, 12(3):373–390, 2016.

[30] Antonio Bayés de Luna, Philippe Coumel, and Jean François Leclercq. Ambulatory sudden cardiac death: mechanisms of production of fatal arrhythmia on the basis of data from 157 cases. *American heart journal*, 117(1):151–159, 1989.

[31] Martyn P Nash, Chris P Bradley, Peter M Sutton, Richard H Clayton, Panny Kallis, Martin P Hayward, David J Paterson, and Peter Taggart. Whole heart action potential duration restitution properties in cardiac patients: a combined clinical and modelling study. *Experimental physiology*, 91(2):339–354, 2006.

[32] Krishnakumar Nair, Karthikeyan Umapathy, Talha Farid, Stephane Masse, Erin Mueller, Radhika V Sivanandan, Kwaku Poku, Vivek Rao, Vidhya Nair, Jagdish Butany, et al. Intramural activation during early human ventricular fibrillationclinical perspective. *Circulation: Arrhythmia and Electrophysiology*, 4(5):692–703, 2011.

[33] Karthikeyan Umapathy, Krishnakumar Nair, Stephane Masse, Sridhar Krishnan, Jack Rogers, Martyn P. Nash, and Kumaraswamy Nanthakumar. Phase mapping of cardiac fibrillation. *Circulation: Arrhythmia and Electrophysiology*, 3(1):105–114, 2010.

[34] Richard A Gray, Arkady M Pertsov, and José Jalife. Spatial and temporal organization during cardiac fibrillation. *Nature*, 392(6671):75, 1998.

[35] Stephanie M Shors, Alan V Sahakian, Haris J Sih, and Steven Swiryn. A method for determining high-resolution activation time delays in unipolar cardiac mapping. *IEEE transactions on biomedical engineering*, 43(12):1192–1196, 1996.

[36] M-A Bray and John P Wikswo. Use of topological charge to determine filament location and dynamics in a numerical model of scroll wave activity. *IEEE transactions on biomedical engineering*, 49(10):1086–1093, 2002.

[37] Pawel Kuklik, Stef Zeemering, Bart Maesen, Jos Maessen, Harry J Crijns, Sander Verheule, Anand N Ganesan, and Ulrich Schotten. Reconstruction of instantaneous phase of unipolar atrial contact electrogram using a concept of sinusoidal recomposition and hilbert transform. *IEEE transactions on biomedical engineering*, 62(1):296–302, 2014.

[38] Caroline H Roney, Chris D Cantwell, Norman A Qureshi, Rasheda A Chowdhury, Emmanuel Dupont, Phang Boon Lim, Edward J Vigmond, Jennifer H Tweedy, Fu Siong Ng, and Nicholas S Peters. Rotor tracking using phase of electrograms recorded during atrial fibrillation. *Annals of biomedical engineering*, 45(4):910–923, 2017.

[39] Pawel Kuklik, Stef Zeemering, Arne van Hunnik, Bart Maesen, Laurent Pison, Dennis H Lau, Jos Maessen, Piotr Podziemski, Christian Meyer, Benjamin Schaffer, Harry Crijns, Stephan Willems, and Ulrich Schotten. Identification of rotors during human atrial fibrillation using contact mapping and phase singularity detection: Technical considerations. *IEEE transactions on bio-medical engineering*, 64:310–318, Feb 2017.

[40] Vincent Jacquemet. A statistical model of false negative and false positive detection of phase singularities. *Chaos: An Interdisciplinary Journal of Nonlinear Science*, 27(10):103124, 2017.

[41] Caroline H Roney, Chris D Cantwell, Jason D Bayer, Norman A Qureshi, Phang Boon Lim, Jennifer H Tweedy, Prapa Kanagaratnam, Nicholas S Peters, Edward J Vigmond, and Fu Siong Ng. Spatial resolution requirements for accurate identification of drivers of atrial fibrillation. *Circulation: Arrhythmia and Electrophysiology*, 10(5):e004899, 2017.

[42] Jacob Laughner, Shibaji Shome, Nicholas Child, Allan Shuros, Petr Neuzil, Jaswinder Gill, and Matthew Wright. Practical considerations of mapping persistent atrial fibrillation with whole-chamber basket catheters. *JACC: Clinical Electrophysiology*, 2(1):55–65, 2016.

[43] Vincent Jacquemet. Phase singularity detection through phase map interpolation: Theory, advantages and limitations. *Computers in biology and medicine*, 102:381–389, 2018.

[44] N. Vandersickel, E. Van Nieuwenhuyse, N. Van Cleemput, J. Goedgebeur, M. El Haddad, J. De Neve, A. Demolder, T. Strisciuglio, M. Duytschaever, and A. V. Panfilov. Directed networks as a novel way to describe and analyze cardiac excitation: Directed graph mapping. *Front. Physiol.,*, 2019.

[45] Laura Martinez-Mateu, Lucia Romero, Ana Ferrer-Albero, Rafael Sebastian, José F Rodríguez Matas, José Jalife, Omer Berenfeld, and Javier Saiz. Factors affecting basket catheter detection of real and phantom rotors in the atria: A computational study. *PLoS computational biology*, 14(3):e1006017, 2018.

[46] Tina Baykaner and Junaid AB Zaman. Another method that shows organization in persistent af? that'sa raap. *Journal of cardiovascular electrophysiology*, 30(12):2713, 2019.

[47] Julien Seitz, Clément Bars, Guillaume Théodore, Sylvain Beurtheret, Nicolas Lellouche, Michel Bremondy, Ange Ferracci, Jacques Faure, Guillaume Penaranda, Masatoshi Yamazaki, et al. Af ablation guided by spatiotemporal electrogram dispersion without pulmonary vein isolation: a wholly patient-tailored approach. *Journal of the American College of Cardiology*, 69(3):303–321, 2017.

[48] Mu Qin, Wei-Feng Jiang, Shao-Hui Wu, Kai Xu, and Xu Liu. Electrogram dispersion–guided driver ablation adjunctive to high-quality pulmonary vein isolation in atrial fibrillation of varying durations. *Journal of cardiovascular electrophysiology*, 31(1):48–60, 2020.

[49] Gonzalo R Ríos-Muñoz, Ángel Arenal, and Antonio Artés-Rodríguez. Real-time rotational activity detection in atrial fibrillation. *Frontiers in physiology*, 9:208, 2018.

[50] Decebal Gabriel Lațcu, Bogdan Enache, Karim Hasni, Ahmed Mostfa Wedn, Naïma Zarqane, Atul Pathak, and Nadir Saoudi. Sequential ultra-high-density contact mapping of persistent atrial fibrillation: An efficient technique for driver identification. *Journal of Cardiovascular Electrophysiology*.

[51] Giorgio Luongo, Luca Azzolin, Massimo W Rivolta, Tiago P Almeida, Juan Pablo Martínez, Diogo C Soriano, Olaf Dössel, Roberto Sassi, Pablo Laguna, and Axel Loewe. Machine learning to find areas of rotors sustaining atrial fibrillation from the ecg.

[52] Prasanth Ganesan, Elizabeth M Cherry, David T Huang, Arkady M Pertsov, and Behnaz Ghoraani. Atrial fibrillation source area probability mapping using electrogram patterns of multipole catheters. *BioMedical Engineering OnLine*, 19:1–23, 2020.

[53] Prasanth Ganesan, Anthony Salmin, Elizabeth M Cherry, David T Huang, Arkady M Pertsov, and Behnaz Ghoraani. Iterative navigation of multipole diagnostic catheters to locate repeating-pattern atrial fibrillation drivers. *Journal of cardiovascular electrophysiology*, 30(5):758–768, 2019.

[54] Max Falkenberg McGillivray, William Cheng, Nicholas S Peters, and Kim Christensen. Machine learning methods for locating re-entrant drivers from electrograms in a model of atrial fibrillation. *Royal Society open science*, 5(4):172434, 2018.

[55] Alexander M Zolotarev, Brian J Hansen, Ekaterina A Ivanova, Katelynn M Helfrich, Ning Li, Paul ML Janssen, Peter J Mohler, Nahush A Mokadam, Bryan A Whitson, Maxim V Fedorov, et al. Optical mapping-validated machine learning improves atrial fibrillation driver detection by multi-electrode mapping. *Circulation: Arrhythmia and Electrophysiology*, 13(10):e008249, 2020.

[56] Jorge G Quintanilla, José Manuel Alfonso-Almazán, Nicasio Pérez-Castellano, Sandeep V Pandit, José Jalife, Julián Pérez-Villacastín, and David Filgueiras-Rama. Instantaneous amplitude and frequency modulations detect the footprint of rotational activity and reveal stable driver regions as targets for persistent atrial fibrillation ablation. *Circulation research*, 125(6):609–627, 2019.

[57] Carlo Pappone, Giuseppe Ciconte, Gabriele Vicedomini, Jan O Mangual, Wenwen Li, Manuel Conti, Luigi Giannelli, Felicia Lipartiti, Luke McSpadden, Kyungmoo Ryu, et al. Clinical outcome of electrophysiologically guided ablation for nonparoxysmal atrial fibrillation using a novel real-time 3-dimensional mapping technique: results from a prospective randomized trial. *Circulation: Arrhythmia and Electrophysiology*, 11(3):e005904, 2018.

[58] Subbarao Choudry, Moussa Mansour, Sri Sundaram, Duy T Nguyen, Srinivas R Dukkipati, William Whang, Paul Kessman, and Vivek Y Reddy. Radar: a multicenter food and drug administration investigational device exemption clinical trial of persistent atrial fibrillation. *Circulation: Arrhythmia and Electrophysiology*, 13(1):e007825, 2020.

[59] Stephan Willems, Atul Verma, Timothy R Betts, Steven Murray, Petr Neuzil, Hueseyin Ince, Daniel Steven, Arian Sultan, Patrick M Heck, Mark C Hall, et al. Targeting nonpulmonary vein sources in persistent atrial fibrillation identified by noncontact charge density mapping: Uncover af trial. *Circulation: Arrhythmia and Electrophysiology*, 12(7):e007233, 2019.

[60] Giuseppe Ciconte, Gabriele Vicedomini, Wenwen Li, Jan O Mangual, Luke McSpadden, Kyungmoo Ryu, Massimo Saviano, Raffaele Vitale, Manuel Conti, Žarko Ćalović, et al. Non-paroxysmal atrial fibrillation mapping: characterization of the electrophysiological substrate using a novel integrated mapping technique. *EP Europace*, 21(8):1193–1202, 2019.

[61] Shohreh Honarbakhsh, Ross J Hunter, Waqas Ullah, Emily Keating, Malcolm Finlay, and Richard J Schilling. Ablation in persistent atrial fibrillation using stochastic trajectory analysis of ranked signals (star) mapping method. *JACC: Clinical Electrophysiology*, 5(7):817–829, 2019.

[62] Neal K Bhatia, Albert J Rogers, David E Krummen, Samir Hossainy, William Sauer, John M Miller, Mahmood I Alhusseini, Adam Peszek, Erin Armenia, Tina Baykaner, et al. Termination of persistent atrial fibrillation by ablating sites that control large atrial areas. *EP Europace*, 22(6):897–905, 2020.

[63] M Swerdlow, M Tamboli, MI Alhusseini, N Moosvi, AJ Rogers, G Leef, PJ Wang, A Rillig, J Brachmann, WH Sauer, et al. Comparing phase and electrographic flow mapping for persistent atrial fibrillation. *Pacing and Clinical Electrophysiology*, 42(5):499–507, 2019.

[64] Tobias G Oesterlein, Axel Loewe, Gustavo Lenis, Armin Luik, Claus Schmitt, and Olaf Doessel. Automatic identification of reentry mechanisms and critical sites during atrial tachycardia by analyzing areas of activity. *IEEE Transactions on Biomedical Engineering*, 65(10):2334–2344, 2018.

[65] Anthony J Salmin, Prasanth Ganesan, Kristina E Shillieto, Elizabeth M Cherry, David T Huang, Arkady M Pertsov, and Behnaz Ghoraani. A novel catheter-guidance algorithm for localization of atrial fibrillation rotor and focal sources. In *2016 38th Annual International Conference of the IEEE Engineering in Medicine and Biology Society (EMBC)*, pages 501–504. IEEE, 2016.

[66] Vijay S Chauhan, Atul Verma, Sachin Nayyar, Nicholas Timmerman, George Tomlinson, Andreu Porta-Sanchez, Sigfus Gizurarson, Shouvik Haldar, Adrian Suszko, Don Ragot, et al. Focal source and trigger mapping in atrial fibrillation: randomized controlled trial evaluating a novel adjunctive ablation strategy. *Heart rhythm*, 17(5):683–691, 2020.

[67] Hartwig Anzt, Felix Bach, Stephan Druskat, Frank Löffler, Axel Loewe, Bernhard Y Renard, Gunnar Seemann, Alexander Struck, Elke Achhammer, Piush Aggarwal, et al. An environment for sustainable research software in germany and beyond: current state, open challenges, and call for action. *arXiv preprint arXiv:2005.01469*, 2020.

[68] Enid Van Nieuwenhuyse, Teresa Strisciuglio, Giuseppe Lorenzo, Milad El Haddad, Jan Goedgebeur, Nico Van Cleemput, Christophe Ley, Alexander V Panfilov, Jan de Pooter, Yves Vandekerckhove, et al. Evaluation of directed graph-mapping in complex atrial tachycardias. *JACC: Clinical Electrophysiology*, 2021.

[69] Nele Vandersickel, Alexandre Bossu, Jan De Neve, Albert Dunnink, Veronique MF Meijborg, Marcel AG van der Heyden, Jet DM Beekman, Jacques MT De Bakker, Marc A Vos, and Alexander V Panfilov. Short-lasting episodes of torsade de pointes in the chronic atrioventricular block dog model have a focal mechanism, while longer-lasting episodes are maintained by re-entry. *JACC: Clinical Electrophysiology*, 3(13):1565–1576, 2017.

[70] Enid Van Nieuwenhuyse, Laura Martinez-Mateu, Javier Saiz, Alexander V Panfilov, and Nele Vandersickel. Directed graph mapping exceeds phase mapping in discriminating true and false rotors detected with a basket catheter in a complex in-silico excitation pattern. *Computers in Biology and Medicine*, 133:104381, 2021.

[71] Gernot Plank, Axel Loewe, Aurel Neic, Christoph Augustin, Yung-Lin Huang, Matthias A.F. Gsell, Jorge Sanchez Elias Karabelas, Mark Nothstein, Anton J Prassl, Gunnar Seemann, and Edward J Vigmond. The openCARP simulation environment for cardiac electrophysiology. pages under review, bioRxiv preprint available, 2021.

[72] Wenzel Kaltenbacher, Markus Rottmann, and Olaf Dössel. An algorithm to automatically determine the cycle length coverage to identify rotational activity during atrial fibrillation – a simulation study. *Current Directions in Biomedical Engineering*, 2(1):167–170, 2016.

[73] G Michael Vincent, MD. The molecular ggenetics of the long qt syndrome: Genes causing fainting and sudden death. *Annual review of medicine*, 49(1):263–274, 1998.

[74] Y. Asano, J. M. Davidenko, W. T. Baxter, R. A. Gray, and J. Jalife. Optical mapping of drug-induced polymorphic arrhythmias and torsade de pointes in the isolated rabbit heart. *J Am Coll Cardiol*, 29(4):831–842, Mar 1997.

[75] Bum-Rak Choi, Francis Burton, and Guy Salama. Cytosolic ca2+ triggers early afterdepolarizations and torsade de pointes in rabbit hearts with type 2 long qt syndrome. *J Physiol*, 543(Pt 2):615–631, Sep 2002.

[76] N. el Sherif, E. B. Caref, H. Yin, and M. Restivo. The electrophysiological mechanism of ventricular arrhythmias in the long qt syndrome. tridimensional mapping of activation and recovery patterns. *Circ Res*, 79(3):474–492, Sep 1996.

[77] N. El-Sherif, M. Chinushi, E. B. Caref, and M. Restivo. Electrophysiological mechanism of the characteristic electrocardiographic morphology of torsade de pointes tachyarrhythmias in the long-qt syndrome: detailed analysis of ventricular tridimensional activation patterns. *Circulation*, 96(12):4392–4399, Dec 1997.

[78] Dmitry O Kozhevnikov, Keiji Yamamoto, Dionyssios Robotis, Mark Restivo, and Nabil El-Sherif. Electrophysiological mechanism of enhanced susceptibility of hypertrophied heart to acquired torsade de pointes arrhythmias: tridimensional mapping of activation and recovery patterns. *Circulation*, 105(9):1128–1134, Mar 2002.

[79] Y. Murakawa, K. Sezaki, T. Yamashita, Y. Kanese, and M. Omata. Three-dimensional activation sequence of cesium-induced ventricular arrhythmias. *Am J Physiol*, 273(3 Pt 2):H1377–H1385, Sep 1997.

[80] Kirsten D Schreiner, Frederik Voss, Julia C Senges, Ruediger Becker, Patrizia Kraft, Alexander Bauer, Kamilla Kelemen, Wolfgang Kuebler, Marc A Vos, and Wolfgang Schoels. Tridimensional activation patterns of acquired torsade-de-pointes tachycardias in dogs with chronic av-block. *Basic Res Cardiol*, 99(4):288–298, Jul 2004.

[81] J. C. Senges, L. D. Sterns, K. D. Freigang, A. Bauer, R. Becker, W. Kübler, and W. Schoels. Cesium chloride induced ventricular arrhythmias in dogs: three-dimensional activation patterns and their relation to the cesium dose applied. *Basic Res Cardiol*, 95(2):152–162, Apr 2000.

[82] Mohamed Boulaksil, Jerome G Jungschleger, Gudrun Antoons, Marien J C Houtman, Teun P de Boer, Ronald Wilders, Jet D Beekman, Jos G Maessen, Ferenc F van der Hulst, Marcel A G van der Heyden, Toon A B van Veen, Harold V M van Rijen, Jacques M T de Bakker, and Marc A Vos. Drug-induced torsade de pointes arrhythmias in the chronic av block dog are perpetuated by focal activity. *Circ Arrhythm Electrophysiol*, 4(4):566–576, Aug 2011.

[83] Tae Yun Kim, Yukiko Kunitomo, Zachary Pfeiffer, Divyang Patel, Jungmin Hwang, Kathryn Harrison, Brijesh Patel, Paul Jeng, Ohad Ziv, Yichun Lu, Xuwen Peng, Zhilin Qu, Gideon Koren, and Bum-Rak Choi. Complex excitation dynamics underlie polymorphic ventricular tachycardia in a transgenic rabbit model of long qt syndrome type 1. *Heart Rhythm*, 12(1):220–228, Jan 2015.

[84] Albert Dunnink, Thom R.G. Stams, Alexandre Bossu, Veronique M.F. Meijborg, Jet D.M. Beekman, Sofieke C. Wijers, Jacques M.T. de Bakker, and Marc A. Vos. Torsade de pointes arrhythmias arise at the site of maximal heterogeneity of repolarization in the chronic complete atrioventricular block dog. *Europace*, 2016.

[85] Fadi G. Akar, Gan-Xin Yan, Charles Antzelevitch, and David S. Rosenbaum. Unique topographical distribution of m cells underlies reentrant mechanism of torsade de pointes in the long-qt syndrome. *Circulation*, 105(10):1247–1253, Mar 2002.

[86] Chris D Cantwell, Caroline H Roney, Fu Siong Ng, Jennifer H Siggers, SJ Sherwin, and Nicholas S Peters. Techniques for automated local activation time annotation and conduction velocity estimation in cardiac mapping. *Computers in biology and medicine*, 65:229–242, 2015.